



On the relation between phase-field crack approximation and gradient damage modelling

Christian Steinke¹ · Imadeddin Zreid¹ · Michael Kaliske¹

Received: 2 August 2016 / Accepted: 17 December 2016
© Springer-Verlag Berlin Heidelberg 2016

Abstract The finite element implementation of a gradient enhanced microplane damage model is compared to a phase-field model for brittle fracture. Phase-field models and implicit gradient damage models share many similarities despite being conceived from very different standpoints. In both approaches, an additional differential equation and a length scale are introduced. However, while the phase-field method is formulated starting from the description of a crack in fracture mechanics, the gradient method starts from a continuum mechanics point of view. At first, the scope of application for both models is discussed to point out intersections. Then, the analysis of the employed mathematical methods and their rigorous comparison are presented. Finally, numerical examples are introduced to illustrate the findings of the comparison which are summarized in a conclusion at the end of the paper.

Keywords Microplane model · Gradient damage · Phase-field · Brittle fracture · Concrete failure

1 Introduction

The correlation between phase-field and gradient damage models in failure analysis is of growing interest, due to the very similar structure of both approaches. Though the starting point is distinct, the resulting governing equations are quite similar. Attempts to use the phase-field method as a regularization technique for damage and comparisons between the two approaches are already discussed in the literature

[8, 9, 30]. The paper at hand is focused on clarifying the apparent similarities between the smeared crack approximation by the phase-field method and implicit gradient damage approach. The main aim is to compare the gradient enhanced microplane damage model, presented in [33], and two types of the unsymmetric phase-field model for brittle fracture, that have been introduced in [27]. Both models are studied in detail considering them being typical representatives of two more general classes of formulations, namely the continuum damage approach of material and the numerical approximation of cracks.

Continuum damage mechanics is a method to describe the degradation of material stiffness due to growing of microcracks and other material defects. Damage can be characterized as a scalar parameter in the simplest isotropic case and as a fourth order tensor in the very general anisotropic case. The damage evolution is usually driven by a scalar equivalent strain variable to measure the level of deformation. Due to its simplicity and efficiency, damage mechanics has been employed to model many materials including concrete. However, a persistent problem of damage models within the finite element method is the numerical instability and mesh dependency, which is a manifestation of the ill-posed underlying differential equations of local damage models. This deficiency motivated the use of nonlocal damage approaches. An implicit gradient damage formulation is a type of a nonlocal damage model which is strongly nonlocal and essentially equivalent to the integral type method [23], but it does not require explicit sharing of information between elements, thus it results in a straightforward implementation in finite element codes. Gradient enhancement has been used to regularize both damage as well as plasticity models [34]. Its basic idea is to estimate a nonlocal field using an additional differential equation beside the classical balance of linear momentum. This additional field is usually the counterpart

✉ Michael Kaliske
michael.kaliske@tu-dresden.de

¹ Institute for Structural Analysis, Technische Universität Dresden, Dresden, Germany

of the local strain or other local internal variables. The price to be paid in this case is adding extra degrees of freedom and solving a coupled system of equations.

The numerical simulation of crack evolution is a wide and complex field of research. Beside the formulation of realistic criteria for crack propagation, the major task is to find a robust and universal model for the approximation of the crack itself. For this purpose, the definition of a crack and its characteristics is an auxiliary first step. Considering bulk material, a crack can be defined as the separation of the material by the formation of two opposing surfaces inside the previously solid structure. In the context of continuum mechanics, there are two opposing implementations possible. On the one hand, the crack may be treated as a part of the continuum with a modified relationship between strains and stresses. Basically, the traction free separation of the crack faces as well as the transmission of compressive stresses by means of contact of the crack surfaces have to be modelled. Furthermore, the transmission of shear stresses needs to be considered. Such kind of models may be summarized under the concept of smeared crack approximation. On the other hand, the formation of crack surfaces may be interpreted as additional outer boundaries of the solid that have to be introduced and (re-)meshed. These approaches, commonly known as discrete crack approximations, treat the finite discrete jump in the displacement field that emerges for an opening crack, in a natural manner. Though, special considerations are necessary for cracks under compressive loading, i.e. preventing the crack surfaces from penetration and model a realistic contact behaviour. A detailed discussion on the comparison of smeared and discrete crack approximation approaches can be found in [27].

Both methodologies, the gradient damage model and the phase-field crack model, may be applied to the numerical simulation of concrete structures under static and transient loading. Though, these models do not aim at the modeling of the concrete behaviour in an all-embracing manner, including long term response like creep or dealing with special types of concrete, rather a general mechanism of failure is considered. Although plain concrete, i.e. without reinforcement, is rarely used in engineering structures, there are several reasons to perform experiments on plain concrete samples. The main motivation is to simplify the rather complex response of reinforced concrete structures as much as possible to characterize the concrete material properties rather than a complex structural behaviour. This is especially important for the economic calibration of model parameters.

In the following section, an overview of the main characteristics of concrete material behaviour and a detailed discussion on the main failure mechanism in concrete is given. Subsequently, the general ideas and assumptions of the gradient damage and the phase-field model are outlined and discussed in consideration of their application to con-

crete failure in two subsections. Section 3 contains a detailed discussion and comparison of the methods implemented to establish a relation between strain and stress. Moreover, the additional differential equations, which are similar but not identical, are discussed with respect of both their origin and impact on the approaches. Section 4 presents a set of numerical examples to demonstrate the findings of the previous sections. The paper is finalised by a summarizing conclusion.

2 Numerical approximation of softening in concrete

2.1 Characteristics of softening in concrete

Concrete is a heterogeneous material consisting mainly of cement, water and aggregates. It presents a manifold behaviour both in the response to certain loading modes as well as with respect to the velocity at which these loadings are applied. In terms of the European standard specification EN 12390-3:2001 [7], concrete is classified in terms of the peak stress measured in a uniaxial compression test, i.e. the compressive strength.

The setup of these tests is standardized both in terms of the geometry of the test sample, considering either a cubic or a cylindrical specimen, as well as the way and the velocity the loading is applied. In general, the compressive strength measured in such a setup is significantly higher than a comparably measured tensile strength. Actually, simplified approaches often neglect the tensile strength of concrete totally. Nevertheless, the regular failure modes, presented in [7] and depicted in Fig. 1, show, that the evolution of splitting cracks due to the lateral expansion of the specimen leads to a loss of structural integrity. Therefore, the value of the compressive strength obtained in such a standard compression test is strongly related to the resistance against the evolution of cracks, both structural and on the material level. It is important to not confuse the compressive strength with another failure mechanism dedicated to compressive loading, i.e. the collapse of pores in the bulk material due to a hydrostatic pressure, because the peak value of stress obtained in such a case is significantly higher.

One of the main aspects of nonlinear behaviour in concrete can be summarized under the concept of softening. In



Fig. 1 Regular failure modes in a compression test according to [7]. **a** Cubic specimen. **b** Cylindrical specimen

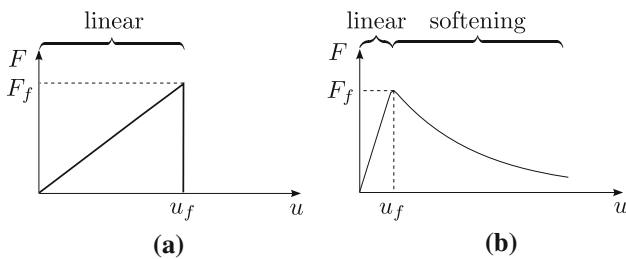


Fig. 2 Relation between deformation and tensile force. **a** Brittle failure. **b** Damage

general, softening describes the reduction of the value of a reaction force that is related to a certain amount of deformation measured at a structural level. The starting point for bulk concrete is the linear elastic relationship between strains and stresses at the material level. This becomes manifest in a linear relation between deformation and forces on the structural level. With respect to the so-called strength of the material, this relationship changes with increased deformation. When the strength is reached, the reaction force that results out of an increased deformation will decrease. This change in the relation of forces and deformation may be as pronounced in brittle fracture examples (Fig. 2a) or continuously in typical damaged structural responses (Fig. 2b).

Both types of softening are related to the same failure mechanism, i.e. the evolution of cracks. In damage approaches, there are microcracks evolving. Especially in concrete, they are expected to be initiated at the weak point of the material, i.e. the bond between mortar matrix and aggregates. Starting from a number of such initiation points, they are supposed to reduce the effective cross-section in a representative volume which results in a macroscopically decreased stiffness. In these terms, the damage variable is a local measurement of the ratio between initial and effective cross-section, that is used to modify the relationship between strains and stresses on the material level. Furthermore, damage approaches are mostly phenomenological, i.e. the evolution of damage is governed by constitutive laws which are motivated, but not strictly defined, by the physical processes governing microcrack evolution. Rather they represent a certain experimentally observed characteristic by a set of arbitrarily chosen equations. The use of more complex equations in addition with more variables to adjust the results to the experimental findings may enhance the model in the scope of the results of previously evaluated experiments. Yet, the prediction, especially beyond the scope of experimental phenomena, is at least questionable.

At this point, a different approach may be promising. Instead of using constitutive equations to describe observed phenomena, the physical process, i.e. the formation of cracks, is modelled especially. In terms of concrete, brittle fracture has to be described. For the numerical implementation

within the finite element method, the task is twofold. At first, a suitable model to approximate the crack has to be chosen. Basically, two approaches exist, namely discrete and smeared crack approximations. Due to the apparent similarities between damage models and smeared crack approximation, the phase-field method is chosen in here. The second important aspect is the implementation of realistic criteria for crack initiation, propagation, kinking, branching and arrest. Again, the phase-field model presents a promising all-embracing approach for these features. Instead of the formulation of phenomenological criteria, e.g. separately for initiation, propagation and branching e.g. by a strength value, stress intensity factor and material force, respectively, the phase-field model provides an energetic formulation that is able to model all kinds of crack evolution in a thermodynamical consistent manner.

Although, concrete is categorized to be brittle in nature, equivalent to other similar materials like rocks or ceramics, the damage-like softening obtained in some situations may contradict the theory of brittle fracture. In brittle fracture, as soon as there are cracks, no transmission of tensile forces over the crack surfaces is present. This results in catastrophic failure of the whole structure, if there are no additional structural load bearing capabilities available, i.e. the reaction force, that results out of a deformation exceeding a critical value, is zero. Nevertheless, at this point the combination of brittle fracture evolution and a typical damage-like softening behaviour is possible. Consider the heterogeneous composition of any concrete structure and also the fact, that in slow loading situations the cracks will start at and propagate along the interface between mortar and aggregates. The result is a rough surface with plenty potential for interlocking. So even though the cracks evolved and separated the specimen in numerous pieces in the worst case, the interlocking of these surfaces represents the possibility for residual load bearing capability of the entire structure, i.e. a damage-like softening behaviour.

2.2 Gradient damage formulation

As a typical representative of continuum damage models, the gradient enhanced microplane damage model, as it was already presented in [24, 33], is discussed. The formulation is based on the gradient enhancement of the equivalent strain. The strong form equations of the problem are the balance of linear momentum

$$\rho \ddot{\mathbf{u}} - \operatorname{div} \boldsymbol{\sigma} = 0 \quad (1)$$

and a modified HELMHOLTZ equation considering the nonlocal equivalent strain

$$\bar{\eta}_m - c \nabla^2 \bar{\eta}_m = \eta_m. \quad (2)$$

Here, σ is the CAUCHY stress tensor, η_m is the local equivalent strain, $\bar{\eta}_m$ is its nonlocal counterpart and c is the gradient activity parameter. div and ∇^2 are the divergence and the LAPLACE operator, respectively. Furthermore, ρ is the density and $\ddot{\mathbf{u}}$ is the vector of acceleration.

In the microplane approach presented here, the relationship between strains and stresses at the GAUSS point level results out of a homogenization of the constitutive relation between strains and stresses on the microplanes under consideration of the damage variable. The homogenization of the results on the microplanes with respect to the macro level of the GAUSS points is realized by the integration over a whole sphere Ω . Therefore, the macroscopic energy function reads

$$\Psi^{mac} = \frac{3}{4\pi} \int_{\Omega} \Psi^{mic} d\Omega. \quad (3)$$

According to [4], the integration is sufficiently accurate if computed with 42 microplanes. Due to symmetries, it is sufficient to use 21 microplanes as follows

$$\frac{3}{4\pi} \int_{\Omega} (\cdot) d\Omega = \sum_{mic=1}^{21} (\cdot) w^{mic}, \quad (4)$$

where w^{mic} is the weight for each integration point according to [33].

At first, the strain tensor $\boldsymbol{\epsilon}$ is projected to the 21 microplanes, where it is decomposed into a volumetric and a deviatoric part, $\boldsymbol{\epsilon}_V$ and $\boldsymbol{\epsilon}_D$, respectively. The decomposition utilizes the normal vector \mathbf{n} on each microplane by defining

$$\boldsymbol{\epsilon}_V = \frac{1}{3} \mathbf{1} \cdot \boldsymbol{\epsilon} \quad (5)$$

and

$$\boldsymbol{\epsilon}_D = \mathbf{n} \cdot \left[\frac{1}{2} \left(\mathbf{I} + \mathbf{I}^T \right) - \frac{1}{3} \mathbf{1} \otimes \mathbf{1} \right] \cdot \boldsymbol{\epsilon} \quad (6)$$

with the help of the second and fourth order identity tensor, $\mathbf{1}$ and \mathbf{I} , respectively.

The free energy at the microplane level including rate-dependency as proposed in [22] reads

$$\begin{aligned} \Psi^{mic} = & \left(1 - d^{mic} \right) \left\{ \frac{1}{2} K^{mic} \epsilon_V^2 \right. \\ & \left. + G^{mic} \boldsymbol{\epsilon}_D \cdot \boldsymbol{\epsilon}_D \left[1 + c_2 \ln \left(\frac{2 \dot{\gamma} s_{cr}}{c_0} \right) \right] \right\} \end{aligned} \quad (7)$$

with the elasticity parameters

$$K^{mic} = 3K \quad (8)$$

and

$$G^{mic} = G, \quad (9)$$

where K and G are the compression and shear modulus, respectively. Here, the scalar damage parameter d^{mic} is implemented, which is uniformly applied to the deviatoric and the volumetric part of Ψ^{mic} . The strain rate magnitude reads

$$\dot{\gamma} = \sqrt{\frac{1}{2} \dot{\boldsymbol{\epsilon}} : \dot{\boldsymbol{\epsilon}}}, \quad (10)$$

evaluating the rate of the strain tensor $\dot{\boldsymbol{\epsilon}}$ at the macroscopic level. c_0 and c_2 are the material rate parameters and s_{cr} is the spacing of parallel cracks. The evolution law of the damage parameter is given by

$$d^{mic} = 1 - \frac{\gamma_0}{\gamma^{mic}} \left[1 - \alpha + \alpha e^{\beta(\gamma_0 - \gamma^{mic})} \right], \quad (11)$$

where α represents the maximum degradation of the material, β controls the shape of softening, and γ_0 is the damage threshold. The microplane chosen for the gradient enhancement is the one with the largest equivalent strain

$$\eta_m = \max_{mic=1}^{21} (\eta^{mic}), \quad (12)$$

and its nonlocal counterpart $\bar{\eta}_m$ is governed by the additional gradient enhancement Eq. (2). Moreover, the equivalent strains of the remaining microplanes are modified by the same ratio of the local to nonlocal largest equivalent strain by

$$\bar{\eta}^{mic} = \frac{\bar{\eta}_m}{\eta_m} \eta^{mic}. \quad (13)$$

The local equivalent strain depends on the local strain components according to the modified von MISES equivalent strain equation

$$\eta^{mic} = 3k_1 \epsilon_V + \sqrt{(3k_1 \epsilon_V)^2 + \frac{3}{2} k_2 \boldsymbol{\epsilon}_D \cdot \boldsymbol{\epsilon}_D}, \quad (14)$$

that separates compressive and tensile contributions. Furthermore, it is modified by the ratio $\bar{\eta}_m/\eta_m$ to prevent localization. Here, k_1 and k_2 are calculated with respect to the ratio between the compression strength f_c and the tension strength f_t of concrete

$$k_r = \frac{f_c}{f_t} \quad (15)$$

and POISSON's ratio ν by

$$k_1 = \frac{k_r - 1}{2k_r(1 - 2\nu)} \quad (16a)$$

and

$$k_2 = \frac{3}{k_r(1 + \nu)^2}. \quad (16b)$$

The history variable γ^{mic} , which drives the evolution of the damage, is defined to be the maximum value of the modified equivalent strain reached in the whole loading history on each microplane, reading

$$\gamma^{mic}(t) = \max_{\tau \leq t}(\gamma_0, \bar{\eta}^{mic}(\tau)). \quad (17)$$

Moreover, as the damage variable is calculated for each microplane separately, and for the sake of a physical visualization, a homogenization to yield a representative damage for each GAUSS point is evaluated as

$$d^{hom} = \frac{\frac{3}{4\pi} \int_{\Omega} d^{mic} d\Omega}{\frac{3}{4\pi} \int_{\Omega} d\Omega}. \quad (18)$$

Finally, the stress tensor is defined in a standard way as the partial derivative of the macroscopic energy function reading

$$\sigma = \frac{\partial \Psi^{mac}}{\partial \epsilon}. \quad (19)$$

2.3 Phase-field crack approximation

As typical representatives of smeared crack approximation in continuum mechanics, two types of the unsymmetric phase-field brittle fracture model, as it was already evaluated in [27], are discussed. In contrast to the damage model introduced before, the phase-field model presents a numerical approximation of a displacement discontinuity, i.e. a sharp crack, in a continuous manner in addition with an energetic crack evolution criterion based on the brittle fracture theory of Griffith described in [11].

In the following, the main assumptions for the deduction of the strong form of the phase-field approach are outlined. The principle equations are presented briefly in order to give an overview on the implementation under discussion. For more detailed information on the spectral and the volumetric-deviatoric split of the inner energy and the derivation of the strong form of the phase-field approach in a dynamic context, the reader is referred to [14, 17, 25], respectively.

The dynamic phase-field model originates out of the HAMILTONIAN principle

$$\delta \int_{t_1}^{t_2} \int_{\mathcal{B}} \mathcal{L} dV + \int_{\partial\mathcal{B}} \mathbf{t}^* \cdot \mathbf{u} dA dt = 0 \quad (20)$$

with the LAGRANGIAN density

$$\mathcal{L} = \psi_{kin} - \psi_{eps} - \psi_{dis} \quad (21)$$

considering the energetic contributions of the kinetic energy density

$$\psi_{kin} = \frac{1}{2} \rho \dot{\mathbf{u}} \cdot \dot{\mathbf{u}}, \quad (22)$$

the dissipated energy density

$$\psi_{dis} = \frac{\mathcal{G}_c}{2l} (p^2 + l^2 |\nabla p|^2) \quad (23)$$

and a strain energy density

$$\psi_{eps} = g(p) \psi^+ + \psi^- \quad (24)$$

Here, \mathbf{u} and $\dot{\mathbf{u}}$ are the vectors of displacement and velocity, respectively. \mathcal{G}_c denotes the fracture toughness and l is the regularization length. p denotes the phase-field degree of freedom and $|\nabla p|$ is the norm of the spatial gradient of the phase-field. The decomposition of the strain energy density into ψ^+ and ψ^- allows the identification of the specific part ψ^+ , which is available for dissipation into the formation of new crack surfaces. It is degraded by the degradation function $g(p)$ with respect to the value of the phase-field.

There are two different approaches for the decomposition of the strain energy available in the literature, namely the volumetric-deviatoric split and the spectral decomposition. The volumetric-deviatoric split was first presented in [1] and its implementation is outlined e.g. in [25]. The spectral split was outlined in [21]. The general idea of both approaches is to identify the amount of the strain energy, which is available for crack surface formation in the sense of energetic competition presented by GRIFFITH's theory of brittle fracture in [11].

The degradation function

$$g(p) = (1 - p)^2 \quad (25)$$

constitutes the link between the numerical crack approximation Γ_l and the crack driving amount of strain energy ψ^+ .

The stress tensor σ is defined in a straight forward manner by

$$\sigma = \frac{\partial \psi_{eps}}{\partial \epsilon} = g(p) \underbrace{\frac{\partial \psi^+}{\partial \epsilon}}_{\sigma^+} + \underbrace{\frac{\partial \psi^-}{\partial \epsilon}}_{\sigma^-}. \quad (26)$$

The decomposition of the strain energy leads to the definition of degraded and undegraded parts of the stress tensor, σ^+ and σ^- , respectively.

The surface of a crack Γ is approximated by a regularized functional, i.e.

$$\Gamma \approx \Gamma_l = \int_{\mathcal{B}} \frac{1}{2l} \left(p^2 + l^2 |\nabla p|^2 \right) dV. \quad (27)$$

The manipulation of Eq. (20) leads to the governing strong form equations

$$\rho \ddot{\mathbf{u}} - \operatorname{div} \boldsymbol{\sigma} = 0 \quad (28)$$

and

$$2(1-p)\psi^+ - \frac{\mathcal{G}_c}{l} p + \mathcal{G}_c l \nabla^2 p = 0. \quad (29)$$

The irreversibility of the phase-field evolution at each time t is achieved by substitution of ψ^+ , which is the crack driving force, in Eq. (29). Instead, the history variable

$$\mathcal{H}(t) = \max_{\tau \leq t} (\psi^+(\tau)) \quad (30)$$

is implemented. The correspondent strong form reads

$$2(1-p)\mathcal{H} - \frac{\mathcal{G}_c}{l} p + \mathcal{G}_c l \nabla^2 p = 0. \quad (31)$$

3 Correlation and distinction between cracks and damage

3.1 Degradation of stiffness

In both models, the vector of unknowns is composed of the displacement and an additional degree of freedom. In the gradient damage approach discussed in this paper, the additional degree of freedom is the nonlocal equivalent strain $\bar{\eta}_m$. However, every local variable, that can be associated with damage evolution, may be chosen and the introduction of its nonlocal counterpart is possible. In contrast, the additional variable in the phase-field approach is the phase-field p . Furthermore, the interpretation of the phase-field variable in the context of brittle fracture always is including the numerical measurement of crack surface magnitude.

A fundamental similarity of gradient damage and crack approximation is the reduction of the amount of stress, that is induced by a certain amount of strain. In general, this is associated with the material behaviour. In the context of the phase-field model, it is called the “degradation of the stiffness”, while in the gradient damage approach it is referred to as the “damage of the material”. However, both approaches

present different methods to implement the modified relation between strains and stresses.

In the phase-field approach, the phase-field is, in addition to the numerical approximation of the crack surface, directly employed for the degradation function $g(p)$, that reduces the stiffness. This becomes obvious by taking a look on the correspondent equation, that defines the fourth order material tensor \mathfrak{C} , which governs the relation between strains and stresses by

$$\boldsymbol{\sigma}_{ij} = \mathfrak{C}_{ijkl} \boldsymbol{\epsilon}_{kl}. \quad (32)$$

In both phase-field approaches under discussion, there is the part \mathfrak{C}^+ , which originates from the double partial differentiation of the portion ψ^+ of the strain energy density that is linked to crack evolution. The reduction or degradation of the part \mathfrak{C}^+ by

$$\mathfrak{C} = g(p) \mathfrak{C}^+ + \mathfrak{C}^- = (1-p)^2 \mathfrak{C}^+ + \mathfrak{C}^- \quad (33)$$

represents one part of the implementation of the local energy balance. On the one hand, the increase of p leads to the reduction of \mathfrak{C}^+ by the multiplier $g(p)$ and represents the reduction of the strain energy density ψ_{eps} in the local energy balance in Eq. (20). On the other hand, increasing p yields increased values for the crack surface functional Γ_l in ψ_{dis} , i.e. increasing the amount of dissipated energy in Eq. (20). Therefore, the change of the phase-field affects both the dissipated energy density ψ_{dis} as well as the strain energy density ψ_{eps} in a counterrotating manner. While the increase of the phase-field yields an increase in the amount of dissipated energy density, this is equalised with the degradation of that portion of the strain energy density, which is identified by ψ^+ .

In contrast, in the gradient damage approach, there is a damage variable d^{mic} , that is not identical to the additional degree of freedom. Likewise to the phase-field, d^{mic} has values in the range between 0 and 1, representing the undamaged bulk by $d^{mic} = 0$ and a completely damaged material with $d^{mic} = 1$. In the gradient damage approach discussed here, the link between the additional degree of freedom, i.e. the nonlocal equivalent strain $\bar{\eta}_m$, and the damage variable d^{mic} is governed by a set of two equations, namely the definition of the history variable

$$\gamma^{mic}(t) = \max_{\tau \leq t} (\gamma_0, \bar{\eta}^{mic}(\tau)) \quad (34)$$

and the damage evolution law

$$d^{mic} = 1 - \frac{\gamma_0}{\gamma^{mic}} \left[1 - \alpha + \alpha e^{\beta(\gamma_0 - \gamma^{mic})} \right]. \quad (35)$$

Furthermore, the impact on the relation between strains and stresses is of a different kind in the gradient damage approach.

Applied to the free energy at each microplane level

$$\Psi^{mic} = \left(1 - d^{mic}\right) \left\{ \frac{1}{2} K^{mic} \epsilon_V^2 + G^{mic} \boldsymbol{\epsilon}_D \cdot \boldsymbol{\epsilon}_D \left[1 + c_2 \ln \left(\frac{2 \dot{\gamma} s_{cr}}{c_0} \right) \right] \right\}, \quad (36)$$

the damage leads to a reduction of the stiffness in all directions. Consequently, once the material is damaged, both tensile and compressive stresses are reduced. This is in contrast to the phase-field model, where even for a fully evolved phase-field $p = 1$ an unmodified relation between the strains and stresses remains, that is associated with ψ^- , which is specified in \mathcal{C}^- . For the spectral split of the inner energy, every compressive principal strain results in unchanged compressive principal stress. In the volumetric-deviatoric split, every compressive volumetric strain induces unchanged compressive volumetric stresses. The remaining parts of the strain would result in zero stresses. In contrast, in the microplane approach, the total amount of stresses is reduced with respect to the value of d^{mic} , independent of their sign and direction. Basically, this is consistent with the theory and assumptions behind both approaches. The phase-field is developed to approximate cracks. Therefore, the natural characteristics to be modelled are the transmission of compressive stresses by means of contact as well as the traction free separation of the surfaces under tensile loading. The aspect of shear transmissions over a closed crack is still an issue of ongoing research and is not included in any phase-field approach up to date. In contrast, in the gradient damage approach, the reduction of the effective cross-section, which transmits stresses, is to be represented. Therefore, a reduced stiffness in both compression and tension is the behaviour expected.

Consistently, the evolution of both p and d^{mic} are driven in different ways. As already pointed out, the driving force of the phase-field evolution in Eqs. (29) and (31) is ψ^+ or rather \mathcal{H} , i.e. the largest value of ψ^+ in the history of the simulation. ψ^+ includes strains and stresses, that are expected to be able to create cracks, i.e. tensile principal strains (spectral split) or tensile volumetric strains and deviatoric strains (volumetric deviatoric split). In contrast, in the gradient damage approach, the damage also may be driven by compressive volumetric strains. This represents an important feature of concrete failure, i.e. the collapse of the concrete pores under high hydrostatic pressure. Pore collapse is beyond the scope of the crack approximation approach and its inclusion would require additional modifications, which are not within the coverage of the discussions in this paper. The specific relation between the damage evolution and the strain tensor in the microplane approach is given by a modified equation of the VON MISES equivalent strain reading

$$\eta^{mic} = 3k_1 \epsilon_V + \sqrt{(3k_1 \epsilon_V)^2 + \frac{3}{2} k_2 \boldsymbol{\epsilon}_D \cdot \boldsymbol{\epsilon}_D}, \quad (37)$$

utilizing the scalar value of the volumetric strain ϵ_V and the vector of the deviatoric strain $\boldsymbol{\epsilon}_D$. Furthermore, there are the parameters k_1 and k_2 that govern the difference in the amount of damage that results out of a certain amount of compressive or tensile volumetric strain. The equation used in the microplane model under discussion requires a compressive volumetric strain value that is 3 times larger than a correspondent tensile volumetric strain to result in the same amount of damage.

Furthermore, there is a slight difference in the impact of d^{mic} and p on the element stiffness. While $(1 - d^{mic})$ defines a linear decrease with respect of the damage variable, in the phase-field approach the decrease is quadratic, given by $(1 - p)^2$. Assuming the same distribution of d^{mic} and p , the local element stiffness is always a little bit lower in the phase-field model than in the gradient damage model.

3.2 Additional degree of freedom

Gradient enhancement is applied for the nonlocal approach of the microplane damage model discussed here. The main reason for a nonlocal formulation is to overcome mesh dependency of the results. Therefore, the parameter, that is nonlocal, may be chosen quite liberately. The nonlocal parameter could be a variable that drives the damage law, e.g. equivalent strain or strain tensor, or it could be even the damage variable itself. The nonlocal distribution of the chosen variable is ensured by a modified HELMHOLTZ equation. In the microplane model under discussion here, the local value of the equivalent strain η_m and its nonlocal counterpart $\bar{\eta}_m$ are linked by

$$\bar{\eta}_m - c \nabla^2 \bar{\eta}_m = \eta_m. \quad (38)$$

In the phase-field models discussed, there is also an additional degree of freedom governed by an additional differential equation. One aspect is, similar to the gradient enhancement of the microplane approach, to ensure the non-locality of the solution. Though, the choice of the nonlocal variable is restricted to the phase-field order parameter p . Furthermore, the phase-field has additional functionality. On the one hand, the phase-field, or more precise the volume integral of the phase-field functional in Eq. (27), represents the regularized amount of crack surface Γ_l numerically. On the other hand, the value of the phase-field is directly determining the value of the degradation function $g(p)$ and, therefore, the amount of stiffness degradation, as already discussed in the previous section. The strong form of the differential equation, governing the phase-field, reads

$$p - l^2 \nabla^2 p = \frac{2l}{G_c} (1-p) \mathcal{H}. \quad (39)$$

The strong form equation of the phase-field model has been modified in such a way, that the similarities to the gradient damage approach are clearly visible. At first, consider the parameter c to be equal to l^2 . Then, the left hand side of Eqs. (38) and (39) are identical both in structure and meaning, i.e. governed by a local driving force value on the right hand side in order to distribute a certain quantity over a finite width with respect to a measure of length given by c or l^2 , respectively. But, in terms of the different theoretical assumptions of both approaches, c and l^2 have different roles and constraints. In the damage model, c may be directly connected to a material characteristic, that should be modelled. In terms of its application to concrete, there is a finite width of the damaged zone, that may be related to the size of the aggregates in the concrete matrix. Therefore, the realistic distribution of the damage over that width, which should be determined by the evaluation of special experiments, is ensured by the value of c . This also enables a realistic approximation of the size effect, as has been shown in [3] for a different type of non local microplane models. In contrast, in the phase-field model, the parameter l represents an artificial measure of length, that has two bounds, given theoretically and numerically. On the one hand, the numerical bound is the relation of l and the characteristic length h of the smallest elements in the discretization. As pointed out e.g. in [14], l should be at least twice the characteristic length of the elements, where the phase-field evolves. On the other hand, the second constraint is a theoretical one. As already pointed out before, the phase-field functional is designed to approximate the crack surface numerically. It is shown in [6], that the functional implemented fullfills this constraint for the limit of $l \rightarrow 0$. For such a case, the analytical results of linear elastic fracture mechanics could be obtained. This would involve the size of the fracture process zone to be reduced to infinitely small size, i.e. a point, and furthermore, the fact, that no size effect could be modelled. Actually, this is impossible for numerical simulations due to the relation between element size and length scale parameter. Due to the finite value of l , also the fracture process zone will be of finite width. In consequence, the results of the phase-field model are influenced by the size of the structure under investigation, because the width of the fracture process zone is not sufficiently small compared to the structural dimension. Yet, as l is a purely artifical parameter and lacks the meaning of c , i.e. the representation of a physically motivated length, this is not introducing a proper model to approximate size effect correctly. Nevertheless, the main conclusion should be, that a realistic crack approximation should use elements as small as possible. In consequence, this represents the main difference between c and l^2 . While the first can be used to simulate a material characteristic, e.g. size

effect, in a realistic manner, the second represents a numerical parameter that has to be as small as possible. Furthermore, this yields the main argument to distinguish damage models, e.g. the gradient enhancement microplane model discussed here, from smeared crack approximation with phase-field, even if they look alike on first sight. While the nonlocality of the simulation of damage can be connected to a phenomenological characteristic of the material, the nonlocal results in phase-field is a consequence of the insufficient smallness of the elements in the discretization, i.e. the element size $2h > l \rightarrow 0$.

The right hand side of the Eqs. (38) and (39) show major differences. The evolution of the nonlocal equivalent strain $\bar{\eta}_m$ in the gradient damage model is driven by the local value of the equivalent strain η_m . In contrast, the phase-field evolution is driven by two aspects. First of all, the term $\frac{2l}{G_c} \mathcal{H}$ represents the driving force due to the value of \mathcal{H} in relation to a regularized value of the fracture toughness $\frac{2l}{G_c}$. Here, \mathcal{H} is the amount of strain energy density, that is available for crack evolution locally. Furthermore, the multiplier $(1-p)$ ensures, that the phase-field evolution remains within the limits $0 \leq p \leq 1$. This is especially important for the direct application of the phase-field value onto the degradation function $g(p) = (1-p)^2$. In contrast to the gradient damage model, where the evolution of d^{mic} within the limits $0 \leq d^{mic} \leq 1$ is ensured by Eq. (35) directly, this constraint is included in the governing differential equation implicitly.

Another important numerical feature is already addressed in [10] and analyzed in [8] in the context of a comparison of phase-field and gradient damage, i.e. the broadening of the crack/damage zone. In contrast to the conclusion of the latter paper, even for the phase-field model there are at least two reasons to trigger a lateral growing of the crack. The first occurs in static and dynamic simulations in combination with the history value driven approach discussed before. Generally, it is indicating a branching phenomenon in the subsequent course of the simulation. Nevertheless, it also occurs in simulations, where the time/load step is too large, see e.g. Fig. 10, where the crack tip widened at the end of each load step due to overloading. Another reason for a lateral growth of the crack tip is found in dynamic simulations. It is shown in [27], that the use of the standard NEWMARK time integration method for wave propagation simulations with a phase-field model leads to the radiation of spurious waves at the phase-field boundary. The magnitude of these artificial waves grows unbounded, leads to phase-field evolution lateral to existing cracks and, finally, the total destruction of the simulation in a very short time. As already indicated in [5], the spurious waves can be eliminated by the use of special time integration methods, that reduce high frequency oscillation, e.g. HHT time integration [13].

3.3 Irreversibility

In general, the evolution of fracture and damage is assumed to be an irreversible process. Nevertheless, it should be noted, that there is experimental evidence on the reversibility of brittle fracture in special circumstances, see e.g. [31]. Furthermore, especially for concrete, there is recent research on the development of self-healing, e.g. with the help of bacteria, e.g. [15], or by additional ingredients in the mixture, e.g. [16]. At the moment, the practical use of these phenomena and approaches is rather small and the standard case is an irreversible nature of cracks. Therefore, the evolution of both damage and phase-field is modelled irreversibly. Though, both models approach this task by different means.

In the damage model, irreversibility is ensured by making the scalar value of the damage on the microplane level d^{mic} to either grow or stay constant in every step of the simulation. The value of d^{mic} is governed by Eq. (11), relating it to a set of parameters α , β and γ_0 and the value of a history variable γ^{mic} . The history variable is calculated in Eq. (17) as the maximum of the damage threshold value γ_0 and the largest value of the nonlocal equivalent strain $\bar{\eta}^{mic}$ with respect to the previously calculated steps of the entire simulation. Therefore, d^{mic} is always the result of the maximal “driving force” γ^{mic} and its irreversibility is ensured.

In the literature on phase-field models, there are two approaches available. The first approach, which is outlined by Kuhn et al. [18], implements additionally imposed boundary conditions on the phase-field degree of freedom, as soon as a limiting value, that represents the “fully broken state”, i.e. $p = 1$, has been reached. This allows local recovery of p as long as $p < 1$. The second approach is already pointed out by Eqs. (30) and (31). It is developed by Hofacker [14] and represents the implementation discussed in this paper, because it is closely related to the procedure of the gradient damage model. In analogy to the gradient damage model, a history variable is defined by the maximum value of a certain quantity with respect to previously calculated steps of the simulation. The history variable \mathcal{H} represents the maximum value of the part of the strain energy density ψ^+ , that is related to the evolution of cracks in an energetic sense according to GRIFFITH’s theory of brittle fracture.

The methods in both approaches are similar, i.e. a history variable is implemented with the help of the $\max(\cdot)$ -function taking into account the entire history of the simulation. Nevertheless, there are differences in the motivation of the link between history variable and the evolution of the damage or phase-field, respectively. In the gradient damage model, the relation between d^{mic} and γ^{mic} is a constitutive equation designed to meet a certain phenomenological behaviour of the material. With the help of a set of parameters, this constitutive relation can be calibrated according to experimental results. In contrast, the relation between the phase-field p

and the history variable \mathcal{H} is based on an energetic consideration. \mathcal{H} contains the largest value of ψ^+ and, therefore, the relation of p and \mathcal{H} directly originates out of the postulate of energetic competition in the theory of brittle fracture.

3.4 Thermodynamic consistency

Considering the basic laws of thermodynamics, a dynamic FEM simulation is considered to describe a closed system. The amount of energy, that is introduced into the system by the application of loads will propagate in the structure and is transformed between strain and kinetic energy. Based on the definitions in Eqs. (3), (22) and (24), the global amount of energy is obtained by means of volume integration over the entire structure \mathcal{B} . Therefore, the kinetic energy reads

$$E_{kin} = \int_{\mathcal{B}} \psi_{kin} dV. \quad (40)$$

Furthermore, the amount of strain energy is defined by

$$E_{\varepsilon} = \int_{\mathcal{B}} \psi_{eps} dV \quad (41)$$

for the phase-field model and by

$$E_{\varepsilon} = \int_{\mathcal{B}} \Psi^{mac} dV \quad (42)$$

for the gradient damage model.

Considering fracture and damage, an additional form of energy, i.e. E_{diss} , has to be introduced, namely the amount of energy that is dissipated into the formation of cracks or damage, respectively. In the phase-field framework, an explicit definition is given by

$$E_{diss} = \int_{\mathcal{B}} \psi_{dis} dV. \quad (43)$$

While such an explicit formulation is missing in the theory of the gradient damage model, the numerical example in Sect. 4.3 shows, that the sum of kinetic and strain energy is also reduced by the formation of damage. Therefore, both approaches are thermodynamically consistent.

The summation of the types of energy considered is the amount of total energy

$$E_{tot} = E_{kin} + E_{\varepsilon} + E_{diss}, \quad (44)$$

which is increased by the application of loads. In addition to the energy types mentioned, an all-embracing approach should consider electric, magnetic, chemical and thermal effects, while only the latter may be of interest for simulations in the scope of this paper. Furthermore, especially for fracture

in concrete, plasticity and the radiation of sound are additional types of energy, that may be considered. Nevertheless, neglecting these additional energy types and restraining the theory to kinetics, strain and dissipation due to damage/crack evolution, the amount of E_{tot} has to be equal to the applied work by the loads and constant if no further loads are introduced, in order to model a closed system realistically.

4 Simulations

4.1 Problem solution methods

The simulation of fracture and damage in three-dimensional concrete structures requires a large amount of elements in combination with many loading/time steps. Therefore, most of the subsequently presented simulations make use of a parallel computation approach. All simulations are performed with a user modified version of FEAP 8.4 [28] and the solution of the parallel equation system is obtained by parallel solution methods of PETSC 3.3-p7 [2].

The gradient damage model's element tangent matrix is unsymmetric and is solved in a monolithic scheme, i.e. the vector of unknowns is obtained in a single load/time step. Therefore, the SUPERLU solver [19] is used for static and dynamic simulations.

The element tangent matrix of the phase-field model presented is symmetric, as long as \mathcal{H} increases for each load/time step. As soon as there is unloading, i.e. \mathcal{H} decreases, the tangent becomes unsymmetric and a special solver needs to be applied. Furthermore, the monolithic solution of the phase-field equation system may not converge in case of propagating cracks. First of all, this is only true for static simulations. In dynamic analyses, the mass matrix, as an additional component of the tangent, stabilizes the solution even for crack propagation and enables a stable monolithic solution as long as the time step is chosen appropriately. Nevertheless, considering static problems, a staggered solution scheme is necessary.

The “simple staggered” solution scheme is a two step approach. First, all phase-field degrees of freedom are fixed and the mechanical unknowns are solved. Then, the mechanical unknowns are fixed to the obtained values and the correspondent set of phase-field unknowns is computed. An extension of this algorithm is the “iterated staggered” scheme, where both steps are repeated several times until there is no change in neither the mechanical unknowns nor the phase-field unknowns. The “simple staggered” scheme is very fast, but suffers from a widening of the phase-field crack if the load steps are too big. In contrast, the “iterated staggered” scheme requires a lot of computational time even for small load steps. Furthermore, for small load steps, there is no significant difference in the crack patterns obtained to that of

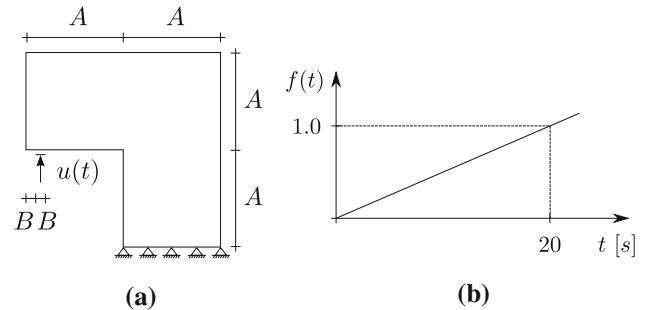


Fig. 3 L-specimen setup. **a** Geometry. **b** Function of load factor

the “simple staggered” scheme. Moreover, the “iterated staggered” scheme obtains widening locally at the position of the crack tip at the end of each load step.

In the subsequent static phase-field simulations, the “simple staggered” scheme with very small load steps is applied. An iterative conjugate gradient solver [12] with a JACOBIAN preconditioner is applied, because the tangent is symmetric for both unknown vectors and only the coupling parts in the monolithic tangent lead to an unsymmetric matrix. In dynamic phase-field simulations, the equation system is solved in a monolithic manner. In order to consider the unsymmetric parts of the tangent at unloading, the Bi-CGSTAB solver [29] is applied.

4.2 L-specimen

The first example investigates the static loading of a concrete structure according to an experiment of WINKLER presented in [32]. The geometry is shown in Fig. 3a, with $A = 250$ mm and $B = 20$ mm. In the experiments, the specimen has a thickness of 100 mm. The displacement loading $u(t)$ is defined by $u(t) = \hat{u} \cdot f(t)$ with $\hat{u} = 1$ mm and $f(t)$ according to Fig. 3b.

The material parameters are elastic modulus $E = 16.5$ GPa and $\nu = 0.18$. The peak load is reached at a displacement $u_p \approx 0.2$ mm in the experiment. The parameters for the microplane model are calibrated to match both the peak load at u_p as well as the softening behaviour observed in the experiment. The correspondent parameters are $\alpha = 0.96$, $\beta = 250$, $\gamma_0 = 2 \times 10^{-4}$, $k_r = 10$, $c = 0.5$ mm 2 , $c_0 = 4 \times 10^{-4}$, $c_2 = 32 \times 10^{-3}$ and $s_{cr} = 0.1$ m. For the phase-field model, the length scale is chosen to be two times the value of the smallest characteristic element length in the mesh, i.e. $l = 2$ mm. The fracture toughness is $G_c = 50$ J/m 2 . The meshes are shown in Fig. 4 and consist of 3774 triangular elements for the damage simulation. The phase-field simulation requires a refined mesh to accurately approximate the crack which results in 62,082 triangular elements.

The damage simulation, abbreviated by “MGD”, is performed for 120 time steps with constant time step size

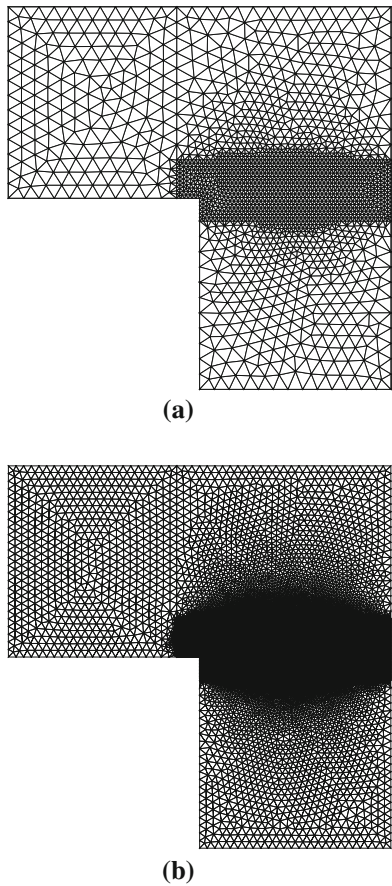


Fig. 4 Triangular meshing. **a** Gradient damage. **b** Phase-field

$\Delta t = 0.1$ s and for all results. The parallel computation is distributed on 8 partitions and took 33 m 22.28 s. The phase-field simulations, abbreviated by “PVD” and “PS” for the volumetric deviatoric split and the spectral split, respectively, both are performed for 50 001 steps, where one step of $\Delta t = 3$ s at the beginning is followed by 50,000 steps with $\Delta t = 0.1$ ms. The parallel computation was distributed on 48 partitions and took 9 h 50 m 30.40 s for the volumetric deviatoric split and 12 h 53 m 42.59 s for the spectral split.

Figure 5 depicts the homogenized damage and the phase-field at the end of the simulation, which generally is in good agreement with the experimentally observed crack pattern. Though, the damage zone only indicates the coarse region, where in the experiment there is evolution of discrete cracks. Nevertheless, the experimentally observed cracks are restricted to the damage zone in the simulation. In the phase-field simulations, it is important to note, that a continuous row of totally degraded elements is obtained along the crack path, which contradicts the analytical solution of the phase-field functional. This was already observed in [27] and results in the overestimation of the calculated crack surface. In consequence, the model’s fracture toughness G_c , that is necessary to simulate the fracture at a displacement of u_p , is lower

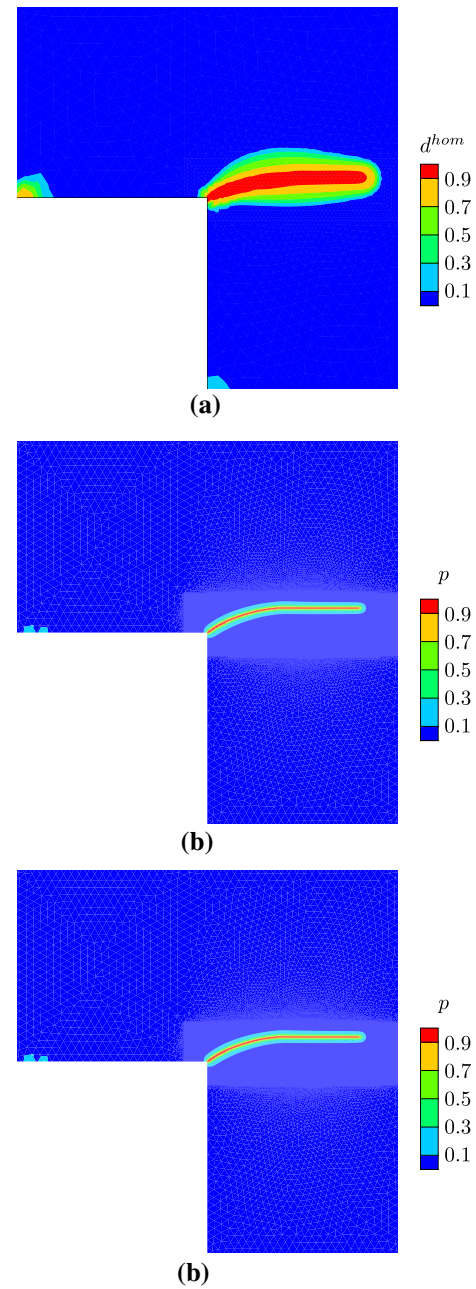


Fig. 5 Final state of damage/crack evolution. **a** MGD, **b** PVD, **c** PS

than the real fracture toughness. Furthermore, Fig. 6 shows the load displacement relation. The gradient damage model shows the typical three stages of (A) initial linear elasticity until $u = 0.08$ mm, followed by (B), a concave decrease in stiffness until $u = 0.35$ mm, i.e. before and after the peak load, is obtained. Then, it shows a characteristic softening behaviour (C), i.e. a slow decrease of the stiffness with a convex shape of the relation between force and displacement. The phase-field model shows additional characteristics, that are typical for brittle fracture. First of all, the linear elastic part (A) reaches close to the peak load. In the volumetric

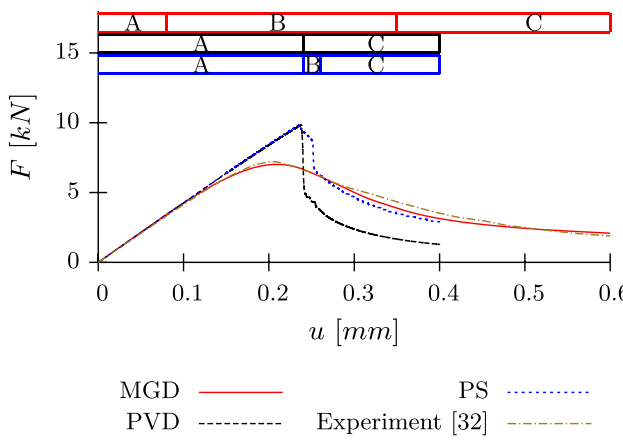


Fig. 6 Load displacement relation

deviatoric split, the part (B) is barely visible. In fact, it is restricted to a very small range of displacements just before the peak load. Then, the reaction force shows a sudden drop, followed by the convex softening part (C) until the end of the simulation. Though, there is a concave softening (B) for the spectral split. Again, it starts just before the peak load is reached, is interrupted by a sudden drop in the reaction force and extends until a second sudden drop in reaction force. From here, the typical softening (C) is obtained until the end of the simulation. In contrast to the smooth softening (C) of the gradient damage model, both phase-field models show a characteristic step-like behaviour. Furthermore, their residual stiffness at the end of the simulation at $u = 0.4$ mm is not the same.

A major difference between the microplane damage model and the phase-field model is the size of the zone, that has a modified stiffness, see Fig. 5. Consistent with the theory, damage is a distributed feature while cracks should be a sharp discontinuity. Nevertheless, phase-field often is related to damage and this may be true, if the requirements of Gamma-convergence, i.e. $l \rightarrow 0$, are omitted and the length scale is increased. In Fig. 7, the initial simulation with the phase-field volumetric deviatoric split is compared to simulations with increased length scale l , i.e. $l = 10$ mm and $l = 20$ mm. First of all, it was not possible to extend the phase-field zone to the size of the damage simulation. For values of $l > 20$ mm, fracture initiated at the bottom boundary instead at the corner of the L-shape, resulting in totally meaningless results. However, the increase of l results in a wider distribution of the zone, where the stiffness is modified by p . Though, Figs. 8 and 9 show, that the characteristic of brittle fracture, i.e. the sudden drop in reaction force, is preserved even for an increased length scale l . This is a significant difference between the approaches damage and crack approximation. Still, increased l also results in a more damage like behaviour before the peak load, i.e. a continuous decrease in stiffness long before the onset of fracture. Furthermore, the increase in l results in a decrease of the value of the peak load.

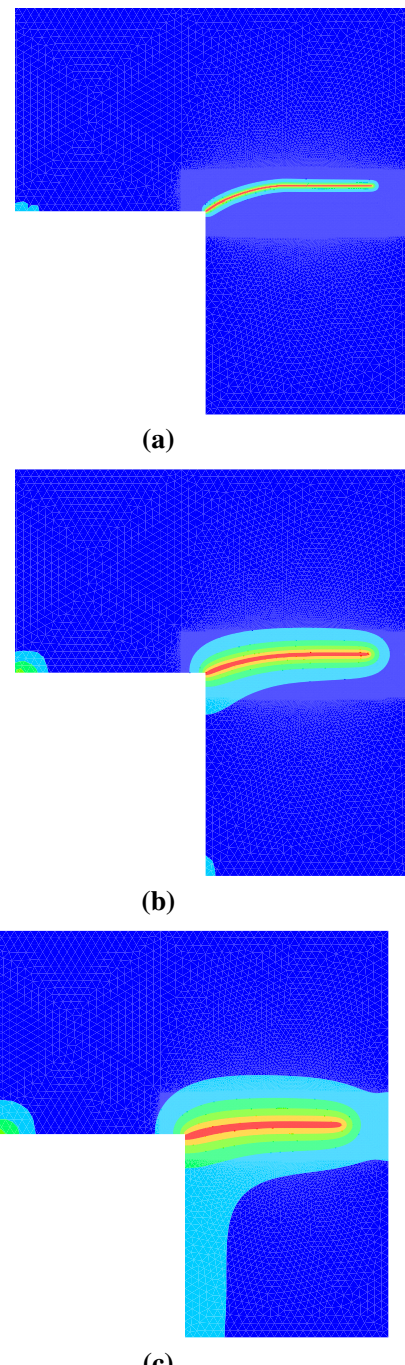


Fig. 7 Phase-field p for PVD with length scale l . **a** $l = 2$ mm **b** $l = 10$ mm **c** $l = 20$ mm

An additional simulation is performed in order to demonstrate the behaviour of the iterated staggered solution scheme for large load steps. The results in Fig. 10 are obtained for a simulation with constant time step $\Delta t = 1$ s. At step four of the simulation, the energetic level at the edge is high enough to trigger phase-field evolution. The iteration between the mechanical field and the phase-field leads to the succes-

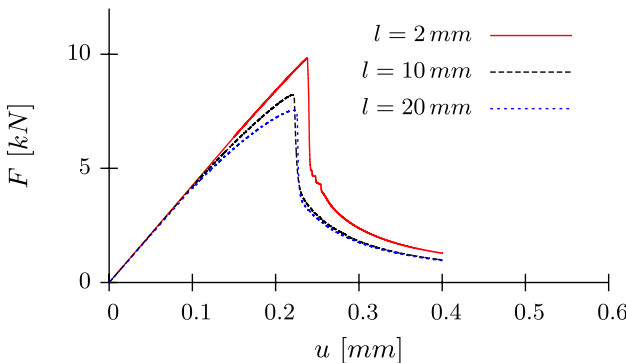


Fig. 8 PVD with different length scale

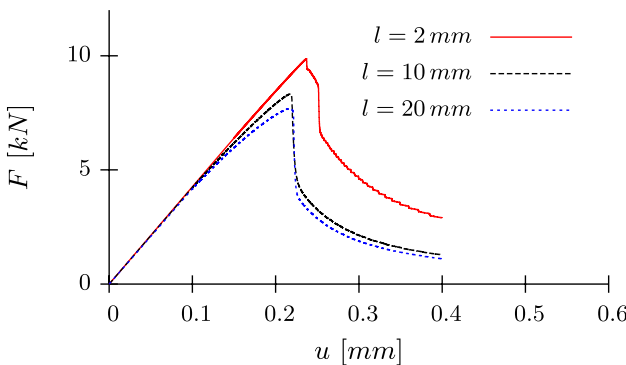
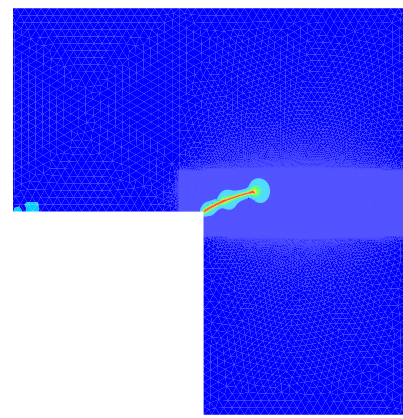


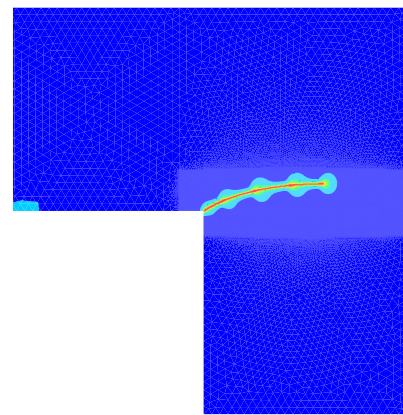
Fig. 9 PS with different length scale

sive propagation of the crack inside one load step. Finally, the phase-field evolution reduces the strain energy level that much, that no further crack propagation is possible. Nevertheless, the stress distribution around the new tip of the crack is large enough, to result in a “bubble”-like shape. Due to the history variable, the shape remains in the subsequent simulation, leading finally to the phase-field pattern to be seen in Fig. 10. Although, the obtained crack pattern is unrealistic and the correspondent relation between load and displacement is totally meaningless, the general direction and coarse path of the crack is correct and indicates the robustness of the method.

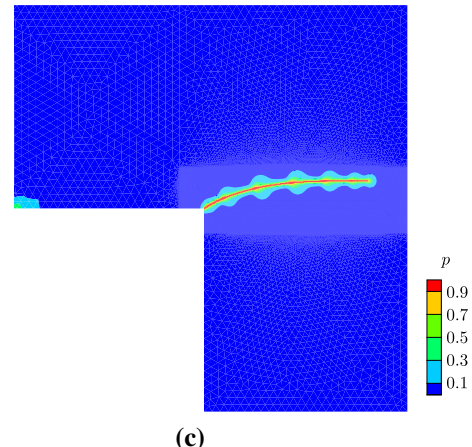
This example shows, on the one hand, that the phase-field approach gives very detailed information about the crack path, where the gradient damage approach identifies a wide region of damaged material. On the other hand, the load displacement relation of the damage model is in perfect agreement with the experimental results, while the phase-field overestimates the peak load and shows an untypical softening behaviour for concrete. Instead of the continuous decrease of stiffness, as obtained with the gradient damage approach, there is sharp crack evolution as soon as the energetic situation provides the correspondent conditions. In combination with the displacement based loading and the NEWTON–RAPHSON iteration scheme to obtain equilib-



(a)



(b)



(c)

Fig. 10 Phase-field p for PVD with too large load steps. **a** $t = 6 \text{ s}$, **b** $t = 8 \text{ s}$, **c** $t = 10 \text{ s}$

rium, this results in a sudden drop in the load displacement relation. Note that, especially after the first drop, numerous equilibrium states are visible, where a slight increase in the force taken by the structure is possible, which are followed then by minor drops that result in a load displacement relation shaped like a stair. As already mentioned, this may be due to the fact, that the phase-field model is applied to

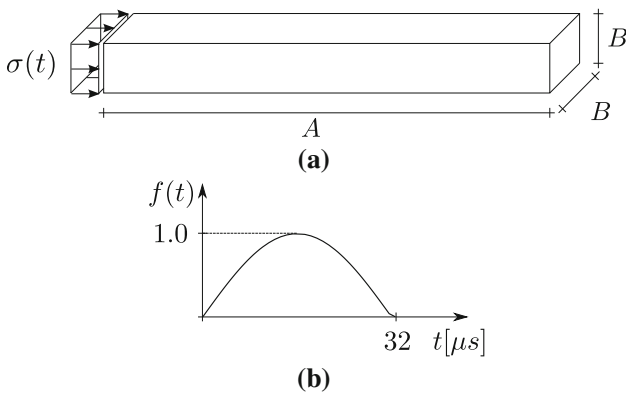


Fig. 11 Spallation test setup **a** Geometry. **b** Function of load factor

a perfectly homogeneous continuum modeling brittle fracture rather than a more realistic composite of aggregates and mortar under consideration of additional mechanisms like viscosity, ductility and interlocking.

4.3 Spallation test

The second example investigates a strongly simplified setup of a split-HOPKINSON-bar spallation experiment in order to study the main mechanism, i.e. the introduction of a compressive wave at the front end of a longish specimen, that results in a tensile wave due to the wave's reflection at the free rear end, which finally leads to spallation of the specimen. Especially in concrete, due to its different strength in compression and tension, such setup is used to investigate the dynamic tensile strength and fracture energy, see e.g. [26]. The setup presented here is simplified such, that only the longitudinal wave propagation is studied in order to demonstrate the ability of both the damage and the phase-field model to simulate spallation in principle. Furthermore, an energetic evaluation is done.

The numerical model is given by a geometry and a loading as shown in Fig. 11 with $A = 200$ mm, $B = 1$ mm, $\sigma(t) = \hat{\sigma} \cdot f(t)$ and $\hat{\sigma} = 1.0$ MPa. The mesh consists of three-dimensional 8 node elements with a constant length of the edge of $h = 1$ mm.

The material parameters are $E = 32$ GPa, $\nu = 0.2$ and $\rho = 2300$ kg/m³. The parameters of the microplane model are $\alpha = 0.98$, $\beta = 650$, $k_r = 14$, $c = 0.001$ mm², $c_0 = 4 \times 10^{-4}$, $c_2 = 32 \times 10^{-3}$ and $s_{cr} = 0.1$ m. With the damage threshold $\gamma_0 = 8 \times 10^{-4}$, the reflected tensile wave creates no damage, therefore this value is used to study the linear elastic behaviour of the model. A second simulation with $\gamma_0 = 8 \times 10^{-6}$ is performed in order to investigate damage evolution. For the phase-field model, the length scale is set to $l = 2$ mm according to the mesh size. The fracture toughness $G_c = 100$ kJ/m² avoids crack evolution, while $G_c = 0.1$ J/m² is used in order to demonstrate the spallation behaviour.

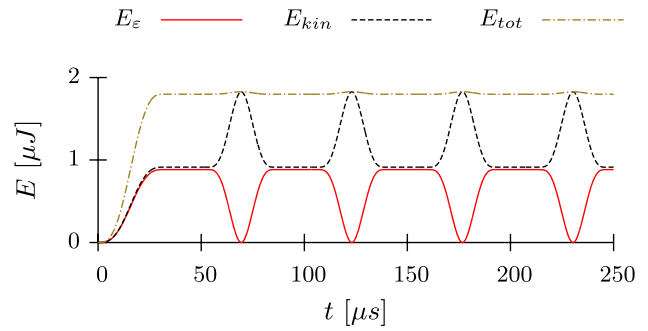


Fig. 12 PS without crack evolution

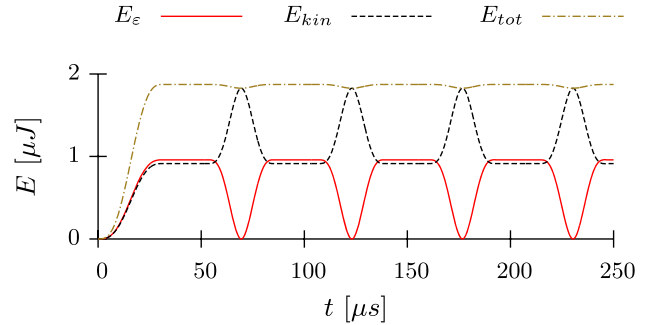


Fig. 13 PVD without crack evolution

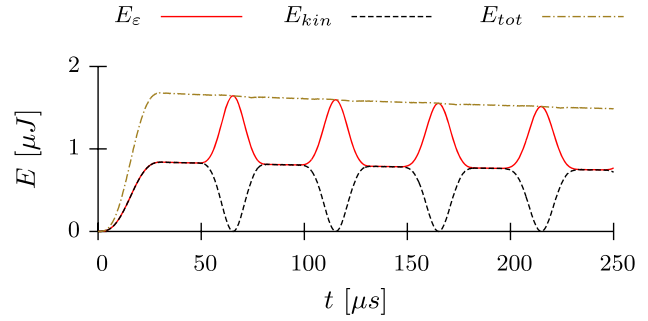


Fig. 14 MGD simulated with NEWMARK ($\beta = 0, 45$ und $\gamma = 0, 80$) without damage evolution

The approximated wave propagation velocity in longitudinal direction is $v_{long} = \sqrt{E/\rho} \approx 3730$ m/s and, therefore, a time of 53.6 μs is needed for the wave to pass through the whole length of the specimen. Every simulation is performed for 1000 transient steps with $\Delta t = 0.25$ μs. Therefore, the wave can run through the specimen at least 4 times. The damage approach is simulated with two different time integration methods, i.e. a NEWMARK time integration scheme with $\beta = 0.45$ and $\gamma = 0.8$ and the HHT time integration with $\rho = 0.667$. The phase-field models are simulated with the HHT time integration with $\rho = 0.667$.

The initial investigation of the linear elastic behaviour of both models for a simple wave propagation setup is evaluated in Figs. 12, 13, 14 and 15. In the period between $t = 0$ μs and $t = 32$ μs, the loading is applied and the total energy

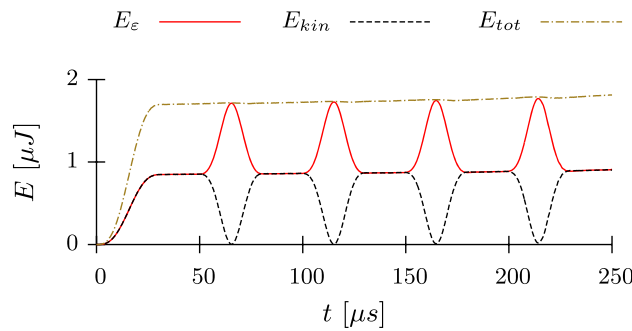


Fig. 15 MGD simulated with HHT ($\rho = 0, 667$) without damage evolution

E_{tot} in the system increases. Because of no crack or damage evolution, the introduced amount of energy is distributed between kinetic and strain energy, E_ε and E_{kin} , respectively. In the special setup of this example, kinetic and strain energy are approximately equal as long as the wave runs through the specimen. When the compressive wave reaches the free end of the specimen, it will be reflected both in sign and direction, i.e. a tensile wave starts to propagate towards the front end. There is a short moment when the wave changes sign and direction, when there is zero stress and strain and the energy is completely stored in movement, i.e. kinetic energy. This is shown e.g. in Fig. 12 at $t = 69.5 \mu\text{s}$, $t = 122.75 \mu\text{s}$, $t = 176.5 \mu\text{s}$ and $t = 230.5 \mu\text{s}$, each time indicating moments in the simulation, where the specimen has its initial length of 200 mm. Moreover, this example can be used to understand movement due to transient loading, i.e. the relation between the local zone of compressed or extended material and the global movement of the specimen. When the stress is applied, the front face of the bar starts to move in longitudinal direction. Therefore, the total length of the specimen decreases until the load is applied totally. Then, a zone of compressed material runs through the bar until its end. Reaching the end, also the rear end is displaced, leading to the increase of the bar's length in excess of the initial length. After that, a zone of extended material runs through the bar until it reaches the front end again. The global result of this mechanism is a bar, that moves in space like a worm in a propulsive manner.

Both phase-field models show a quite good result with respect to energy conservation behaviour when simulated with the HHT time integration method. There are minor numerical errors at the times of wave reflection, i.e. an overestimation of the total energy for the spectral split and an underestimation of the total energy for the volumetric deviatoric split. Nevertheless, the amount of total energy recovers to a constant value each time. In contrast, the damage model shows a slight decrease in total energy when simulated with the NEWMARK time integration. The application of HHT time

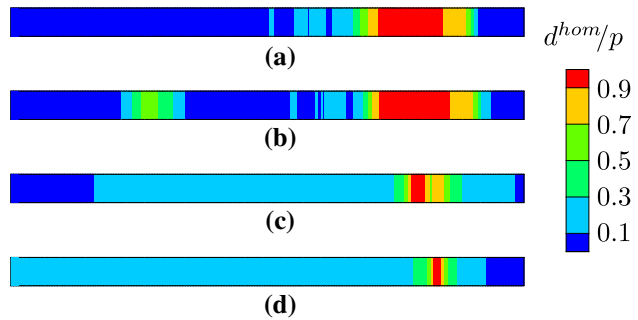


Fig. 16 Spallation test damage $d^{hom}/\text{crack } p$ evolution at $t = 250 \mu\text{s}$. **a** MGD with NEWMARK **b** MGD with HHT, **c** PS, **d** PVD

integration to the damage model results in a slight increase of total energy. Considering the time $t = 32 \mu\text{s}$ to be the reference for E_{tot} , the energy loss is $\approx 11.2\%$ and the energy gain is $\approx 6.8\%$

Figure 16 shows, that all formulations investigated are suitable to model the principle mechanism of spallation, if the parameters are calibrated properly. Therefore, a realistic meshing in combination with detailed experimental data on split-HOPKINSON-bar spallation tests presents the possibility to calibrate the model parameters with respect to dynamic material behaviour in general. In principle, the damaged zone of the gradient model is much larger than the cracked zone in the phase-field models, which is in perfect agreement with the theoretical assumptions of both models. At this point, it should be noted, that it was impossible to obtain a spallation result with the phase-field volumetric deviatoric split and the original setup, i.e. no lateral constraint. Either the fracture toughness is too large to create a spallation at all or the crack is obtained at the front end of the bar where the loading is applied. This is a result of the volumetric deviatoric decomposition of the strain energy density and the assumption, that every deviatoric strain is creating a crack. The longitudinal load in combination with no lateral constraint results in a longitudinal stress which is more than $\approx 13,000$ times larger than the lateral stresses. Therefore, in contrast to the spectral split, most of the energy introduced is considered to be contributing to crack evolution, even for the compressive wave at the beginning. Therefore, the elements are constrained in lateral direction all over the bar, which results in a ratio of ≈ 100 between longitudinal to lateral stresses and the results displayed in Figs. 16d and 18.

The detailed energetic evaluation is presented in Figs. 17, 18, 19 and 20, where the sum of strain and kinetic energy $E_{rev} = E_\varepsilon + E_{kin}$ is introduced. Similar to the linear elastic setup, there is an increase in total energy E_{tot} for the first $32 \mu\text{s}$. For the phase-field spectral split, no crack evolution occurs until the first reflection of the wave at the rear end. The evolving tensile wave results in crack evolution that consists of 4 completely cracked elements, i.e. $p > 0.99$ for all

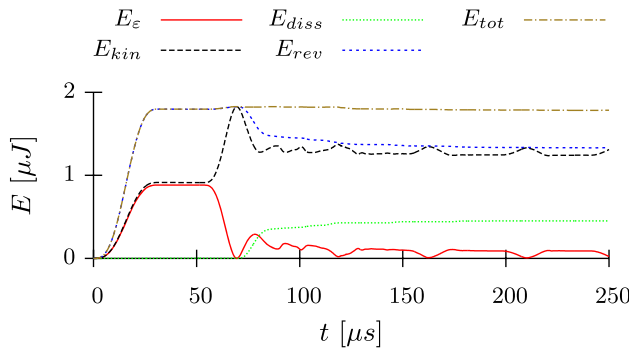


Fig. 17 PS with crack evolution

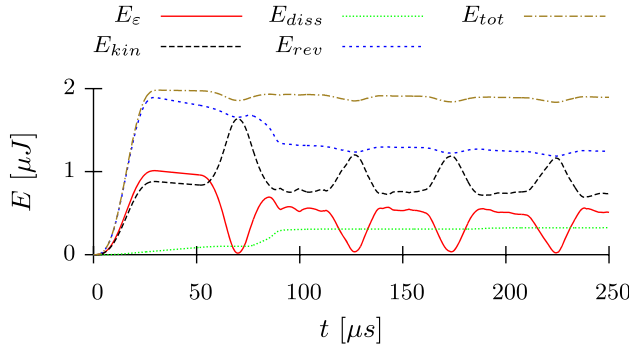


Fig. 18 PVD with crack evolution

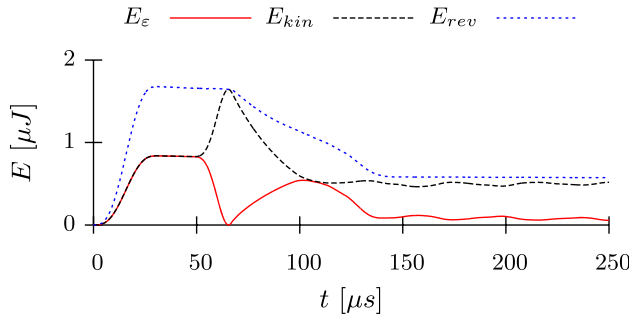


Fig. 19 MGD simulated with NEWMARK and damage evolution

their nodes. This corresponds to a dissipation of $\approx 15\%$ of E_{tot} . Also, the peak value of the tensile stress is reduced to 0.5 MPa, compared to the peak value of the compressive stress of 1.0 MPa. Still, this tensile stress value is large enough to result in a phase-field value of $p > 0.1$ in the regions of the rest of the specimen, resulting in a total amount of dissipated energy of $\approx 25\%$ of E_{tot} . Furthermore, Fig. 17 indicates, that after fracture most of the energy is stored in the kinetic energy E_{kin} , i.e. the movement of the rear bar fraction. In addition, the numerical error observed in the linear elastic setup, i.e. the change of the value of E_{tot} , disappeared after crack evolution.

The behaviour of the phase-field volumetric deviatoric split is totally different. As already indicated, the special setup of this simulation results in the fact, that most of the

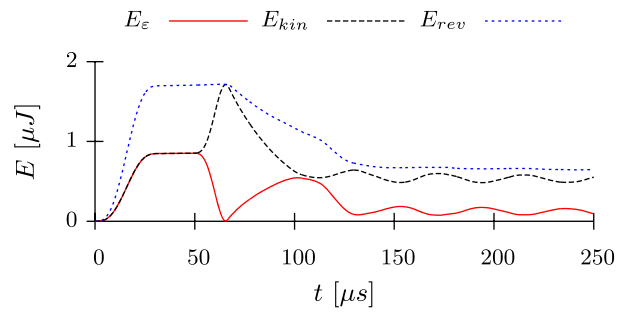


Fig. 20 Gradient damage simulated with HHT ($\rho = 0, 667$) and damage evolution

strain energy is considered to be contributing to crack evolution, regardless of the wave's sign and direction. This is improved by the lateral constraints all over the bar, but still there is dissipation from the beginning of the simulation, i.e. a constant increase in dissipated energy E_{diss} . Nevertheless, also the phase-field volumetric deviatoric split shows a significant increase in dissipation rate after the first reflection of the wave, resulting in a crack evolution that consists of 2 completely cracked elements. After that, the amount of dissipated energy has a constant value of $\approx 17\%$ of E_{tot} . Furthermore, the energetic distribution changes significantly compared to the phase-field spectral split. Instead of having most of the energy stored in the movement of the rear fraction of the bar, $\approx 30\%$ of E_{tot} is stored in E_ε , i.e. runs through the bar as a stress wave.

The energetic evaluation of the spallation simulation results with the gradient damage model displayed in Figs. 16a, b are shown in Figs. 19 and 20, respectively. In the gradient damage model, there is no explicit formulation of the energy, that is dissipated by the evolution of damage. Therefore, the calculation of the total energy, consisting of kinetic, strain and dissipation contributions, is not possible in the straight forward manner of the evaluations of the phase-field simulations. Instead, the linear elastic simulations, Figs. 14 and 15, can be used. Similar to the previous simulations, the total amount of energy increases due to the loading and then stays constant up to the first reflection at $t = 69.5 \mu s$ in both simulations. Then, there is a significant change due to the formation of the damage. Both simulations show, that the amount of energy stored in deformation and movement, i.e. E_{rev} , is decreasing by more than 60% after the damage evolved. Therefore, even though there is no explicit formulation of the dissipated amount of energy, the model is thermodynamically consistent. The amount of energy dissipated depends on the model parameters, especially on the choice of γ_0 , which is the reason that the results of phase-field and damage models are not identical in the energetic sense. Furthermore, Figs. 19 and 20 present a comparison on the time integration methods used. In the linear elastic setup, there are significant amounts of total energy lost

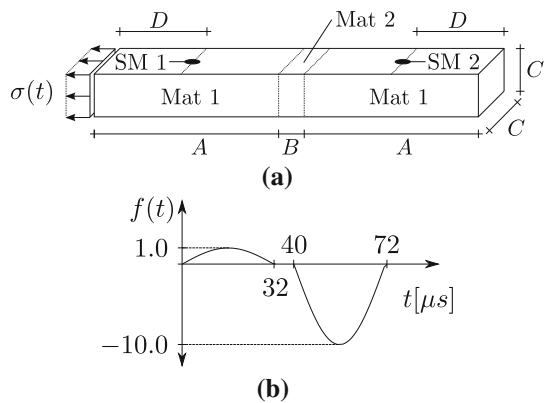


Fig. 21 Alternate load test setup. **a** Geometry. **b** Function of load factor

and introduced for the NEWMARK and HHT time integration method, respectively. After damage evolution there is no further energy loss for the NEWMARK time integration and the HHT time integration method shows a slight loss of energy. Furthermore, the distribution between E_ε and E_{kin} is affected by the time integration. In the simulation with NEWMARK, there is less energy stored in deformation.

The simulations demonstrate the principal capability of both models, to simulate the fundamental mechanism of spallation and points out the differences in the results. Furthermore, the impact of the time integration method is shown for the simulations with the microplane model.

4.4 Alternate loading

The third example is a purely numerical setup to demonstrate a characteristic difference between the phase-field and the microplane approach pointed out in Sect. 3.1. Similar to the previous example, the wave propagation in a thin bar is studied. The bar consists of three parts - a strong part, a short weak part and a strong part. A small tensile stress wave is introduced and runs along the bar. The tensile stress is large enough, to damage/crack the weak material. After a short interval without loading, a compressive wave is introduced. The behaviour of the damaged/cracked “separation” of both strong parts under compressive loading is investigated. Considering a closed crack, compressive loading has to be transmitted by contact. In contrast, damaged material has no stiffness in any direction, therefore a transmission is not possible.

The simulation’s geometry and loading function are shown in Fig. 21 with $A = 230$ mm, $B = 40$ mm, $C = 1$ mm, $D = 125$ mm, $\sigma(t) = \hat{\sigma} \cdot f(t)$ and $\hat{\sigma} = 1.0$ MPa. SM 1 and SM 2 indicate the position, where the magnitude of longitudinal stress is recorded for the evaluation in Figs. 22 and 23. The mesh consists of three-dimensional 8 node elements with a constant length of the edge of $h = 1$ mm.

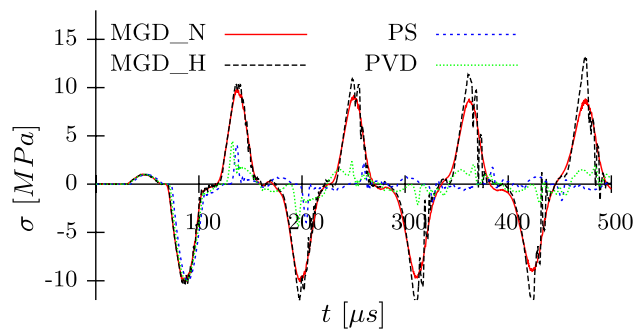


Fig. 22 Stress evaluation at SM 1

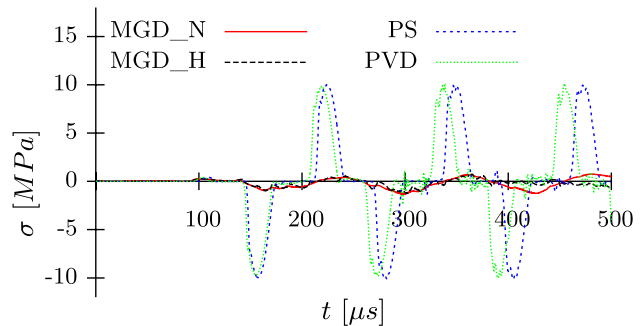


Fig. 23 Stress evaluation at SM 2

The material parameters are $E = 32$ GPa, $\nu = 0.2$ and $\rho = 2300 \frac{\text{kg}}{\text{m}^3}$. The parameters of the damage model are $\alpha = 0.98$, $\beta = 650$, $k_r = 14$, $c = 0.001 \text{ mm}^2$, $c_0 = 4 \times 10^{-4}$, $c_2 = 32 \times 10^{-3}$ and $s_{cr} = 0.1$ m. Material 1 has a damage threshold $\gamma_0 = 8 \times 10^{-4}$ and material 2 has $\gamma_0 = 8 \times 10^{-6}$. In the phase-field simulation, the length scale is $l = 2$ mm. Material 1 has a fracture toughness of $G_c = 10 \text{ kJ/m}^2$ and material 2 has $G_c = 0.1 \text{ J/m}^2$.

The wave propagation speed in longitudinal direction v_{long} is identical to the one in the example before with $v_{long} \approx 3730$ m/s. Therefore, the wave needs $\approx 134 \mu\text{s}$ to run through the whole length of the specimen. Every simulation is performed within 2000 transient steps with $\Delta t = 0.25 \mu\text{s}$. Again, the damage model is simulated with both the NEWMARK time integration scheme with $\beta = 0.45$ and $\gamma = 0.8$ as well as the HHT time integration with $\rho = 0.667$. The phase-field models are simulated with the HHT time integration with $\rho = 0.667$.

The results of the simulations are shown in Figs. 22 and 23 as time plots of the stresses in longitudinal direction at a distance of 125 mm and 375 mm from the point of load application, respectively. The gradient damage simulations are abbreviated with “MGD”, where “_N” indicates NEWMARK time integration and “_H” the HHT time integration. First of all, the small tensile wave triggers the evolution of damage/crack, that is restricted to the zone of weak material, in all four simulations. Furthermore, the time plots show the

characteristics of both methods as expected. For the gradient damage model simulations, after damage evolved, there is a barrier between the two strong parts, which cannot be passed by the compressive wave. Therefore, the compressive wave is reflected again and again in the front strong part until the end of simulation, as indicated in Fig. 22. Though, the stresses in the rear strong part, see Fig. 23, are not totally zero because of two reasons. On the one hand, there is a transmission of a minor tensile wave before the evolution of damage and, on the other hand, the damaged weak material part seems to radiate spurious waves that accumulate during the simulation. This basic behaviour is similar for both time integration methods used. Nevertheless, Fig. 22 also shows a characteristic similar to the spallation example. The longer the simulation is running, the smaller and higher the peak values of the stresses are for the NEWMARK time integration and for the HHT time integration, respectively. The main difference between the damage and the phase-field simulations is shown in Fig. 23, where it is evident, that the compressive wave is transmitted by the phase-field crack. After transmission, the wave is reflected at the rear end, changing in both direction and sign. Reaching again to the crack, the wave, which is in tension now, is reflected again and, therefore, the wave is “trapped” in the rear strong part for the rest of the simulation. Furthermore, there is a significant portion of the wave, that is “trapped” in the front strong part, see Fig. 22. As the initial tension wave triggers the evolution of the crack, it also tears away the rear strong part, i.e. opens the crack. Therefore, the compressive wave first has to close the crack, before any stress can be transmitted. The waves shown in Fig. 22, that are “trapped” in the front strong part, represent exactly that portion of the wave, that is required to close the crack. After the crack is closed, i.e. the local strains are negative, the remaining part of the compressive wave is transmitted.

This example shows a major difference between the phase-field crack approximation and the gradient damage model. While phase-field treats the crack’s abilities to separate under tension and to transmit forces under compression in a natural way, gradient damage is representing a fundamentally different feature. The damage may be triggered by both compression and tension and, therefore, it follows straight forward that the stiffness is reduced in both directions. While this is beneficial, if both failure mechanisms are to be modelled, it may lead to wrong results in special situations like the example presented here. This is especially true for complex dynamic simulations, where multiple wave reflection are present and the behaviour of a structure after failure is of interest, e.g. collapse studies or the investigation of residual load bearing behaviour. It should be noted, that it is possible to formulate damage models with a split between compression and tension damage variables and equivalent strains, e.g. [20], which can capture the above mentioned feature. An accord-

ing extension of the gradient enhanced microplane model is discussed in [35].

5 Conclusions

In the first part of this study, a detailed comparison between the basic assumptions and governing equations for the phase-field model for crack approximation and the nonlocal microplane damage model are presented. In the second part, three numerical examples are studied, in order to demonstrate the findings before.

Both models are multi-field approaches, i.e. extending the set of unknown nodal displacements by an additional degree of freedom. While this is a measure of strain, i.e. the non-local equivalent strain, for the gradient damage model, the additional parameter in phase-field method is the phase-field parameter p , that has multiple functionality in the approach. On the one hand, it is used for the nonlocal numerical approximation of the crack surface and, therefore, enables the objective energetic consideration of GRIFFITH’s surface energy. On the other hand, it is used for a reductive multiplier to modify the stiffness. In the damage approach, the nonlocal equivalent strain is constitutively linked to the damage variable that affects the stiffness. In the phase-field model, the stiffness is reduced in special consideration of direction. Two “energetic splits” are employed, namely the spectral and the volumetric deviatoric decomposition. Based on that, the evolution of cracks is triggered by exceeding a predefined energetic limit, which is the numerical implementation of GRIFFITH’s crack propagation criterion. In the damage model, a constitutive law is governing the link between equivalent strain and damage evolution such, that both tensile failure due to crack evolution and compressive failure due to pore collapse may be described. Consistently, the phase-field reduces the stiffness only in the direction of that parts, that contributed to the crack evolution, while a stiffness reduction in all directions is implemented in the damage model. Both models ensure the irreversibility of damage/crack evolution with the help of a history variable. Furthermore, both models show thermodynamical consistency during and after the evolution process.

Further studies are required for the extension of the phase-field model to a realistic treatment of shear forces in the crack and to model the failure mechanism of pore collapse. Also, a suitable time integration method to simulate symplectic wave propagation in the gradient damage model has to be found. Both models have to be extended by plasticity and creep in order to model all relevant characteristics of concrete.

Acknowledgements The authors would like to acknowledge the financial support of German Research Foundation under grant KA 1163/19 and of ANSYS, Inc, Canonsburg, USA. Furthermore, we thank the Center for Information Services and High Performance Computing (ZIH) at TU Dresden for generous allocations of computer time.

References

1. Amor H, Marigo JJ, Maurini C (2009) Regularized formulation of the variational brittle fracture with unilateral contact: numerical experiments. *J Mech Phys Solids* 57:1209–1229
2. Balay S, Abhyankar S, Adams MF, Brown J, Brune P, Buschelman K, Dalcin L, Eijkhout V, Gropp WD, Kaushik D, Knepley MG, McInnes LC, Rupp K, Smith BF, Zampini S, Zhang H, Zhang H (2016) PETSc Web page. <http://www.mcs.anl.gov/petsc>
3. Bažant P (1990) Non local microplane model for fracture, damage and size effect in structures. *J Eng Mech* 116:2485–2505
4. Bažant ZP, Oh BH (1986) Efficient numerical integration on the surface of a sphere. *Z Angew Math Mech* 66:37–49
5. Borden MJ (2012) Isogeometric analysis of phase-field model for dynamic brittle and ductile fracture. Ph.D. thesis, The University of Texas, Austin
6. Braides A (2002) Gamma-convergence for beginners. Oxford University Press, Oxford
7. DIN EN 12390-3:2001 (2002) Prüfung von Festbeton Teil 3: Druckfestigkeit von Probekörpern. Beuth Verlag GmbH, Berlin
8. de Borst R, Verhoosel CV (2016) Gradient damage versus phase-field approaches for fracture: similarities and differences. *Comput Methods Appl Mech Eng*
9. Duda FP, Ciarbettini A, Sánchez PJ, Huespe AE (2015) A phase-field/gradient damage model for brittle fracture in elastic–plastic solids. *Int J Plast* 65:269–296
10. Geers M, de Borst R, Brekelmans W, Peerlings R (1998) Strain-based transient-gradient damage model for failure analyses. *Comput Methods Appl Mech Eng* 160:133–153
11. Griffith AA (1921) The phenomena of rupture and flow in solids. *Philos Trans R Soc Lond Ser A* 221:163–198
12. Hestenes MR, Stiefel E (1952) Methods of conjugate gradients for solving linear systems. *J Res Natl Bur Stand* 49:409–436
13. Hilber H, Hughes T, Taylor R (1977) Improved numerical dissipation for the time intergration algorithms in structural dynamics. *Earthq Eng Struct Dyn* 5:283–292
14. Hofacker M (2013) A thermodynamically consistent phase field approach to fracture. Ph.D. thesis, Universität Stuttgart, Stuttgart
15. Jonkers H (2011) Bacteria-based self-healing concrete. *Heron* 56(1/2):1–12
16. Kanellopoulos A, Qureshi T, Al-Tabbaa A (2015) Glass encapsulated minerals for self-healing in cement based composites. *Constr Build Mater* 98:780–791
17. Kuhn C (2013) Numerical and analytical investigation of a phase field model for fracture. Ph.D. thesis, Technische Universität Kaiserslautern, Kaiserslautern
18. Kuhn C, Müller R (2011) A new finite element technique for a phase field model of brittle fracture. *J Theor Appl Mech* 49:1115–1133
19. Li XS (2005) An overview of SuperLU: algorithms, implementation, and user interface. *ACM Trans Math Softw (TOMS)* 31:302–325
20. Mazars J (1990) A description of micro-and macroscale damage of concrete structures. *Eng Fract Mech* 25:729–737
21. Miehe C, Welschinger F, Hofacker M (2010) Thermodynamically consistent phase-field models of fracture: variational principles and multi-field fe implementations. *Int J Numer Methods Eng* 83:1273–1311
22. Ožbolt J, Sharma A, Reinhardt HW (2011) Dynamic fracture of concrete–compact tension specimen. *Int J Solids Struct* 48:1534–1543
23. Peerlings RHJ, Geers MGD, de Borst R, Brekelmans WAM (2001) A critical comparison of nonlocal and gradient-enhanced softening continua. *Int J Solids Struct* 38:7723–7746
24. Qinami A, Zreid I, Fleischhauer R, Kaliske M (2016) Modeling of impact on concrete plates by use of the microplane approach. *Int J Non-Linear Mech* 80:107–121
25. Schlüter A (2013) FE-Implementierung eines dynamischen Phasenfeldmodells für Bruchvorgänge. Master's thesis, Technische Universität Kaiserslautern, Kaiserslautern
26. Schuler H (2004) Experimentelle und numerische untersuchungen zur schädigung von stoßbeanspruchtem beton. Ph.D. thesis, Universität der Bundeswehr München, München
27. Steinke C, Özenc K, Chinaryan G, Kaliske M (2016) A comparative study of the r-adaptive material force approach and the phase-field method in dynamic fracture. *Int J Fract* 201:1–22
28. Taylor RL Feap—a finite element analysis program. <http://www.ce.berkeley.edu/projects/feap/>
29. van der Vorst HA (1992) Bi-cgstab: a fast and smoothly converging variant of Bi-CG for the solution of nonsymmetric linear systems. *SIAM J Sci Stat Comput* 13:631–644
30. Voyatzis GZ, Mozaffari N (2013) Nonlocal damage model using the phase field method: theory and applications. *Int J Solids Struct* 50:3136–3151
31. Wiederhorn SM, Townsend PR (1970) Crack healing in glass. *J Am Ceram Soc* 53:486–489
32. Winkler B, Hofstetter G, Niederwanger G (2001) Experimental verification of a constitutive model for concrete cracking. *Proc Inst Mech Eng J Mater Des Appl* 215:75–86
33. Zreid I, Kaliske M (2014) Regularization of microplane damage models using an implicit gradient enhancement. *Int J Solids Struct* 51:3480–3489
34. Zreid I, Kaliske M (2016) An implicit gradient formulation for microplane drucker–prager plasticity. *Int J Plast* 83:252–272
35. Zreid I, Kaliske M (2016) Microplane modeling of cyclic behavior of concrete: a gradient plasticity-damage formulation. *Proc Appl Math Mech* 16:415–416